Experimental study of trailing-edge bluntness noise reduction by porous plates

John R. Kershner* and Justin W. Jaworski[†] Lehigh University, Bethlehem, PA, 18015, USA

Thomas F. Geyer[‡]

formerly: Technical Acoustics Group, Brandenburg University of Technology Cottbus - Senftenberg, now with: Institute of Electrified Aero Engines, German Aerospace Center (DLR), 03046 Cottbus, Germany

Porosity is investigated as a means to mitigate trailing-edge bluntness noise. Inspired by nature's silent flier, the owl, porosity has been shown in previous theoretical and experimental works to be effective in the reduction of turbulence noise scattered by edges, where a single dimensionless parameter controls the influence of porosity on the sound field. The present work examines experimentally the acoustics of porous plates characterized by this same dimensionless porosity parameter in a wind tunnel, where special attention is paid to the acoustic power scaling on flight speed and associated changes in directivity. A phased microphone array and subsequent beamforming analysis enable the collection of detailed source maps near the porous edge, and radially-spaced microphones measure the directivity changes of the generated noise. Results show strong tonal peaks due to edge bluntness that can be reduced with increasing porosity parameter. Further acoustic results are presented and compared across a range of dimensionless porosity parameter values with varying hole geometries.

I. Nomenclature

c = speed of sound c_l = chord length f = frequency

H = boundary layer thicknessOSPL = overall sound pressure level, dB

R = pore radius

Re = Reynolds number based on c_l s = hole-to-hole center spacing SPL = sound pressure level, dB

St = Strouhal number

U = characteristic flow speed U_0 = freestream velocity

 U_{rms} = root-mean-square of velocity x = streamwise Cartesian coordinate y = spanwise Cartesian coordinate

Y = spanwise width

z = vertical Cartesian coordinate

 α_h = open area fraction

 γ = acoustic power exponent of U

^{*}PhD Student, Mechanical Engineering and Mechanics, jrk520@lehigh.edu, Student Member AIAA

[†]Associate Professor, Mechanical Engineering and Mechanics, jaworski@lehigh.edu, Associate Fellow AIAA

[‡]Senior Researcher, German Aerospace Center (DLR), thomas.geyer@dlr.de, Member AIAA Member

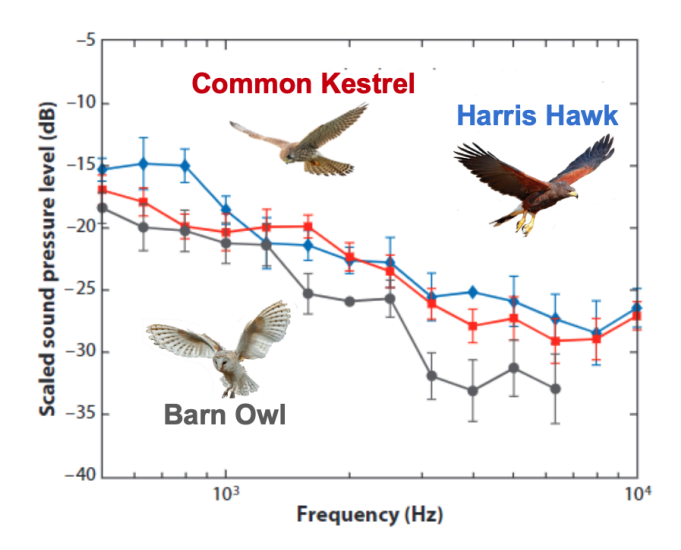


Fig. 1 Owl flyover noise comparison to other birds. Adapted from [1, 3].

II. Introduction

Noise measurements of live animals indicate that owls fly quieter than other birds [1]. A comparison of flyover noise from various birds in Fig. 1 shows how ovel flight animals in the contraction of flyover noise from various birds in Fig. 1 shows how ovel flight animals in the contraction of flyover noise from various birds in Fig. 1 shows how ovel flight animals in the contraction of flyover noise from various birds in Fig. 1 shows how ovel flight animals in the contraction of flyover noise from various birds in Fig. 1 shows how ovel flight animals in the contraction of flyover noise from various birds in Fig. 1 shows how ovel flight animals in the contraction of flyover noise from various birds in Fig. 1 shows how ovel flight animals in the contraction of flyover noise fly from various birds in Fig. 1 shows how owl flight noise is significantly lower at high frequencies. This quiet flight is caused in part by the tattered fringe at the trailing edge (TE) of their wings. This edge feature has been idealized by wing porosity [2], which has been shown to reduce flow noise in a laboratory setting using guidance from theoretical analyses [3, 4]. The early theoretical and numerical work of Howe [5] on porous plate acoustics modeled a point vortex passing over a trailing edge to show that the presence of perforations could reduce trailing-edge noise significantly, and computational simulations by Khorrami & Choudhary [6] indicated that the presence of porosity on a flat plate can reduce sound by reducing the strength of the edge scattering and by modifying the hydrodynamic noise source itself.

Further experiments investigated the acoustic and aerodynamic effects of fully and partially porous airfoils in an aeroacoustic wind tunnel with a microphone array and force-balance setup to measure changes in lift and drag [1, 7, 8]. These experiments used porous SD 7003 airfoils composed of various foams where the presence of porosity reduced noise up to 10 dB for frequencies less than 10,000 Hz. The reductions in noise depended strongly on the flow resistivity of the porous medium, and these porous airfoils generated excess noise at frequencies above 10,000 Hz, which may be due to flow interactions with surface roughness [7, 8]. Later theoretical works modeled chordwise-varying porosity inspired by the flow resistivity of owl wings in aerodynamic [9, 10] and acoustic [11, 12] contexts, where the latter found that varying the hole distribution can lead to greater noise reductions than the case of uniform porosity. These studies also showed changes in directivity due to porosity and overall reductions, however, the model could not account for roughness noise, which is a significant sound source for realistic wings.

In addition to categorizing porosity by flow resistivity, more recent studies have chosen porous designs by their acoustic impedance. In Jiang [13], porosity characteristics such as hole size and spacings were selected based off of characteristic acoustic impedance and the absorption coefficient, as measured in an impedance tube using the transfer function method first discussed in [14, 15]. Their study found that porous edge extensions reduced low frequency noise but increased noise at higher frequencies, except when paired with serrations, which are known to successfully decrease high frequency noise [16].

Porous designs can be catered to reduce specific types of tonal noise. In Showkat Ali et al. [17], porous treatments are investigated to reduce bluntness noise, which they found to be prevalent at St = 0.20, a fundamental vortex shedding frequency. In the best case, they found that highly permeable materials could reduce the peak tonal noise by 35 dB [17], but this reduction in noise depended highly on the percentage of porous material and permeability. They also found that the use of porous edges helped to reduce the flow acceleration over the edge which is thought to lead to a weakening of the vortex shedding. While the work of [8] and [17] showed how porosity can successfully reduce overall noise and bluntness noise, there is still more work to be done to investigate how porosity and porous geometries affect the acoustic power scaling on flow speed for bodies in a flow.

The acoustic power scaling of the radiated sound on flow speed, U^{γ} , varies from $5 \le \gamma \le 6$ for porous edges and non-compact airfoils [2, 8], which is to be compared against the $\gamma = 5$ result for impermeable edges [18]. In Chen et al. [4], a time-domain Green's function approach is used to solve the problem of a vortex ring passing over a semi-infinite porous plate to predict the acoustic power scaling, directivity patterns, and acoustic pressure waveforms. Their theoretical model uses a dimensionless porosity parameter,

$$\delta = \frac{2\alpha_h c}{\pi^2 f R},\tag{1}$$

which was identified by Ffowcs Williams [19] in his analysis of infinite porous surfaces and was later used by Jaworski & Peake [2] to show that the acoustic scaling of porous edge noise on flight speed becomes U^6 for large values of δ , which results in an effective decrease of noise in low-Mach-number flows. In this equation, α_h is the open-area fraction, c is the speed of sound, f is the frequency, and R is the pore radius. This change in acoustic power scaling is accompanied by a notable change in sound directivity, from a cardioid to a dipole shape [4]. Experiments at the Applied Research Laboratory at the Pennsylvania State University were the first to experimentally investigate this parameter δ as a means to describe porosity and how it affects scattered sound. Preliminary results from a vortex-ring setup in a quiescent fluid show favorable changes in directivity and sound power at different values of δ [20, 21]. However, a companion experiment to confirm these results in a moving fluid flow using boundary-layer turbulence as the acoustic source is currently lacking.

The purpose of this paper addresses this shortcoming and examines experimentally the sound field from porous plates in a fluid flow over a range of dimensionless porosity parameter values. Changes in sound pressure levels and directivity will be measured in complement to the central focus on the reduction of edge bluntness noise engendered by porous edges. The effects of pore geometry and patterns to the acoustic field are also analyzed.

III. Methods

The experimental apparatus uses 0.17 m (chord length) × 0.30 m (span width) × 0.003 m (thickness) acrylic plates that are designed with various hole shapes and spacings to span the range of δ . The parametric range of δ is determined from the theoretical analysis of Chen et al. [4] to span from the impermeable to the highly-porous limiting behaviors of porous edge noise. Because the δ value was originally developed for the case of a single vortex passing over an edge with a single frequency, its use to describe the porosity of plates experiencing turbulent-boundary-layer TE noise must be slightly adapted. The δ must instead be calculated for each frequency, and therefore there is an effective range for which each plate was designed. Specifically, the plates were designed to achieve noise reductions in the 300 Hz to 4,000 Hz range, and are categorized by groupings of low, medium, and high porosity, where each group has the same theoretical δ at the same frequency.

To investigate how changes in geometry might affect the generated noise and associated directivity, circular and square holes with both aligned and offset pore patterns are investigated and manufacturing is done by laser cutting. The hydraulic radius is taken for the R term in δ in the case of square holes. Table 1 lists the plates in this experimental program and their corresponding features. The low parameter plates, labeled starting with L, enable δ in Zone 1 in Fig. 2, the medium parameter plates, labeled starting with M, enable δ in Zone 2 in Fig. 2, and the high parameter plates, labeled starting with H, enable δ in Zone 3 in Fig. 2. Lastly, there is a fully impermeable plate for reference comparison.

The measurements were conducted in the small open jet aeroacoustic wind tunnel that the Brandenburg University of Technology (BTU) in Cottbus, Germany [22]. Fig. 3 shows a photograph of the experimental setup. The nozzle in the experiments has a rectangular exit area with dimensions of $0.23 \text{ m} \times 0.28 \text{ m}$ and enables a maximum flow speed of approximately 50 m/s. Attached to the upper and lower edge of the nozzle were rectangular side plates made of acrylic glass. These side plates were equipped with approximately 12 mm wide strips of *anti slip tape* to force transition and thus ensure the presence of a turbulent boundary layer over the plates. Similar to the setup used in [23], circular rotatable discs were set into the side plates. The flat plates under examination were mounted at both ends to these circular discs, which allow adjustment of the angle of attack.

Constant Temperature Anemometry (CTA) measurements were performed at a distance of 0.09 m from the nozzle exit to analyze the flow field it supplies. This distance corresponds to the location of the flat plate leading edges in the acoustic measurements. The velocity profile at this location was found to be uniform, with a very low turbulence intensity of approximately 0.3 % at the center point (see Fig. 4).

The acoustic measurements were performed with 11 1/4th inch free-field microphones located on an arc at one side of the test section and with a planar microphone array located at the opposite side along one wall of the test section. The data were recorded with a sampling frequency of 51.2 kHz and a duration of 40 s and stored on a RAID system. Post processing was performed using the open source Python package *Acoular* [24]. For the measurements

Table 1 Test plate information

Plate name	Hole type	R, mm	s, mm	α_h
L1	Circular aligned	0.9	12.5	0.016
L2	Circular unaligned	0.9	12.5	0.016
L3	Square aligned	0.9	19.5	0.0086
L4	Square unaligned	0.9	19.5	0.0086
M1	Circular aligned	0.9	5.0	0.10
M2	Circular unaligned	0.9	5.0	0.10
M3	Square aligned	0.9	8.0	0.051
M4	Square unaligned	0.9	8.0	0.051
H1	Circular aligned	0.9	4.0	0.16
H2	Circular unaligned	0.9	4.0	0.16
Н3	Square aligned	0.9	4.9	0.13
HΔ	Sauare unaligned	0.0	4 9	0.13

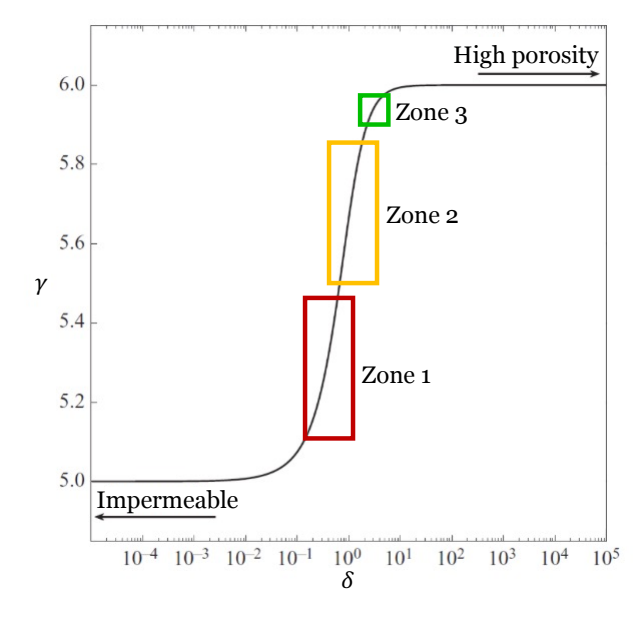


Fig. 2 Acoustic power scaling vs. porosity parameter. Zone 1: plates L1 to L4, Zone 2: plates M1 to M4, Zone 3: plates H1 to H4. Adapted from the analysis of Chen et al. [4].

with the single microphones, the time data were transferred to the frequency domain using a Fast Fourier Transform (FFT) according to Welch's theorem [25], which was done on Hanning-windowed blocks with a size of 4096 samples with an overlap of 50 %. The results were then converted to sound pressure levels with a reference value of 20 μ Pa. For the measurements with the planar microphone array, the same FFT settings were used, and delay-and-sum (DAS) beamforming was calculated using *Acoular* to extract the noise source location and magnitudes. 6 dB is subtracted from the beamforming result to account for the reflection at the rigid array, thus leading to results that correspond to the value a single microphone would measure at the center of the array.

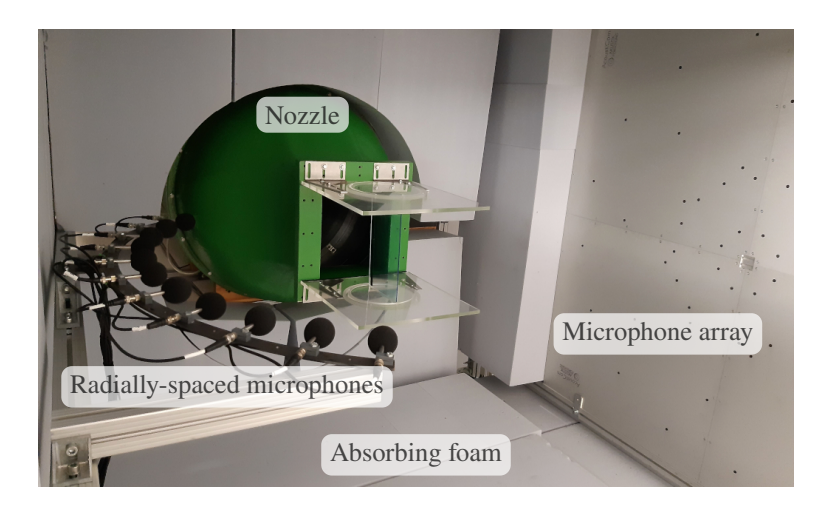


Fig. 3 Photograph of the experimental setup inside the aeroacoustic wind tunnel

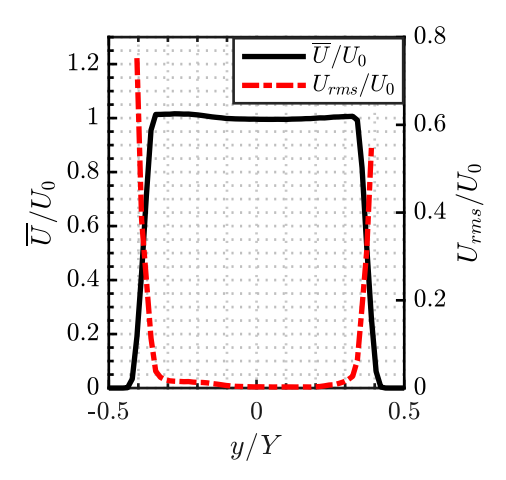


Fig. 4 Flow conditions at the location of the leading edge of the plates $(\overline{U}/U_0 \text{ and } U_{rms}/U_0 \text{ for } U_0 = 20 \text{ m/s})$

IV. Results

A. Sound pressure level spectra

Results are shown and discussed for the impermeable reference plate and the perforated plates shown in Table 1. The flow velocities ranged from 9 m/s < U_0 < 40 m/s which yields an estimated chord based Reynolds number of 1.01×10^5 < Re < 4.50×10^5 . Frequency-domain spectra from the center microphone of the radially-spaced array (see Fig. 3) for the impermeable plate at all flow speeds are shown in Fig. 5a. These spectra have sharp tonal peaks that increase in frequency with increasing flow speeds. The SPL spectra are then plotted against Strouhal number (St) based off TE thickness in Fig. 5b, which shows that the peaks align at approximately St = 0.20. This is similar to findings from [13, 17], and within the range of 0.12 < St < 0.22 found in [26]. Beamforming results for the impermeable plate at U_0 = 35 m/s at the f of the tonal peak are shown in Fig. 6. The soundmap is shown using a 3 dB dynamic range, and the dominant noise source for this frequency is at the plate TE. The beamforming results help to confirm the TE bluntness as being the source of the tonal peaks as the area of highest magnitude aligns nearly perfectly with the TE.

Fig. 7 shows spectra recorded from the center microphone vs. St at a selected flow velocity, $U_0 = 25$ m/s, for the low, medium, and high porosity groupings of plates. With increasing porosity come increasing reductions of the bluntness noise peak. The high porosity plates in Fig. 7c are successful at reducing the low-frequency noise, below the frequency of the noise peak, and can reduce the peak by up to 20 dB. These reductions come at a cost, however, as there is an increase in high-frequency noise, likely due to the the perforations acting as roughness elements. The

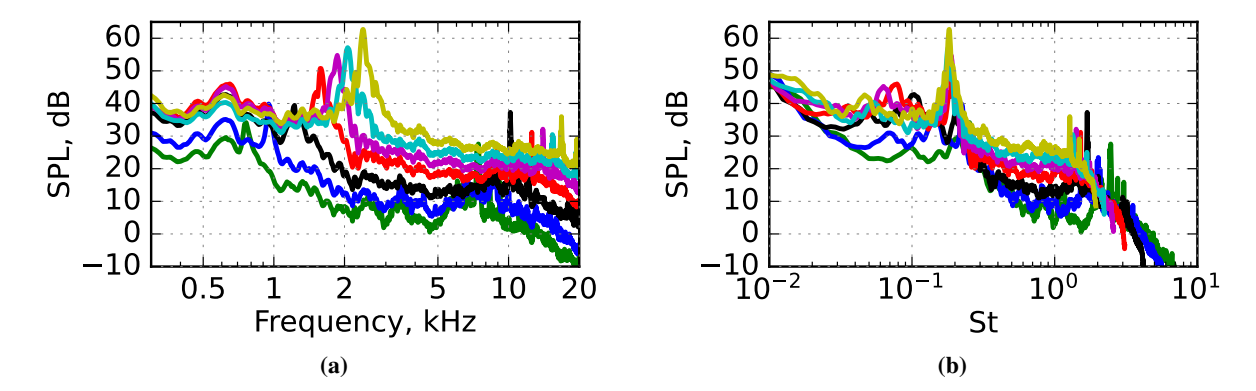


Fig. 5 Dependence of sound pressure level on (a) frequency and (b) St for an impermeable plate at all tested flow speeds (9 m/s—, 13 m/s—, 18 m/s—, 25 m/s—, 30 m/s—, 35 m/s—, 40 m/s—).

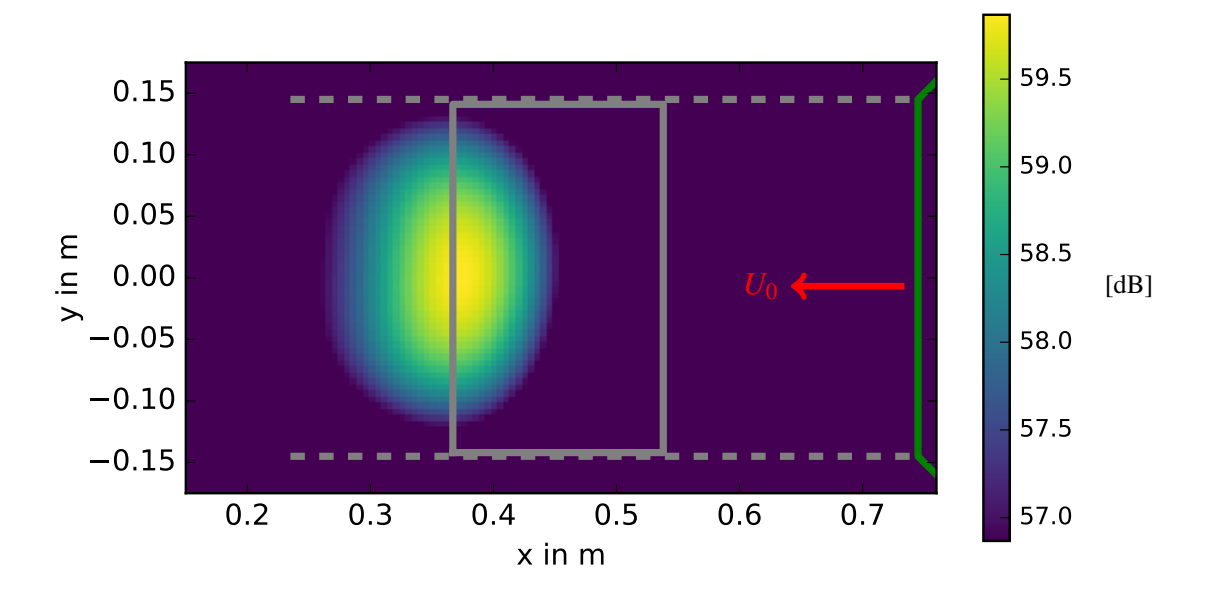


Fig. 6 DAS beamforming at bluntness noise peak single frequency f = 2,100 Hz for impermeable plate (——) at $U_0 = 35$ m/s in wind tunnel with side plates (——) and nozzle (——). Flow direction right to left.

attenuation at low frequencies and the bluntness noise peak reduces with reducing porosity. The low-porosity plates in Fig. 7a barely reduce the low frequency noise and do not reduce the bluntness noise peak, and the results for the medium porosity plates in Fig. 7b are in between that of the low and high porosity plates. The trend of porosity reducing low-frequency noise at approximately 300 Hz to 2,000 Hz but increasing high-frequency noise beyond 2,000 Hz is seen at all flow speeds. There are also strong tonal peaks at St = 1.6 in Fig. 7. The origin of this noise could be the wind tunnel fan itself or the interaction of the flow with parts of the nozzle or the side plates. As previous investigations using the same wind tunnel did not feature these tones, and as they are probably of aerodynamic origin due to the constant Strouhal number, it is likely that they are produced by the flow interacting with parts of the setup. However, further research is necessary to confirm this.

The different hole geometries have an affect on the noise spectra as well. In general, the plates with circular perforations were more successful at reducing the bluntness noise peak. For the high porosity set, the plates with square holes reduce lower-frequency noise but very slightly increase the high frequency noise (see Fig. 7c). The opposite is true for the medium and low porosity plates where the circular holes reduced the most low frequency noise but also produced more high frequency noise (see Figs. 7a and 7b). It was hypothesized in this study that offsetting the holes

in the flow direction (plates L2, M2, and H2) may lead to a reduction in roughness noise due to the possibility of the upstream turbulence to dissipate before reaching the next hole; however, no meaningful difference was found between plates of aligned and offset holes of the same porosity.

B. Changes to overall sound pressure levels (OSPLs) and directivity

The overall sound pressure level (OSPL) is defined as:

OSPL =
$$10 \log_{10} \left(\sum_{i} 10^{\text{SPL}_i/10 \text{ dB}} \right) \text{dB},$$
 (2)

where SPL_i is the sound pressure level at each frequency band from 300 Hz to 20,000 Hz calculated using the process described in the Methods section. Changes to OSPL are first shown in Fig. 8 where the maximum reduction in OSPL due to porosity is approximately 3 dB by plates H1 and H2. This relatively small reduction in OSPL is due to the porous plate creating excess roughness noise at high frequencies. While plates H1 and H2 (with circular holes) were the most successful of the high porosity grouping, the overall performance of the plates in the medium and low porosity grouping varied greatly with hole geometry and U_0 , as M4 performed slightly better than M2 at high velocities, but this ranking shifted at lower velocities.

This trend of slight reductions in noise can be further visualized by polar plots of OSPL calculated at all 11 radially spaced microphone locations. Fig. 9 shows the OSPL for the reference plate and porous plates L2, M2, and H2 at different U_0 . The porous plate H2 is able to reduce the OSPL at all measured angles and flow speeds; however, plates M2 and L2 have mixed results depending on flow speed and location. Fig. 10 shows the SPL of the bluntness noise peak at St = 0.20 for a given U_0 and clearly illustrates how increasing porosity, from plates L2, to M2, to H2, leads to increased reduction of the bluntness noise peak.

V. Summary

A testing program to evaluate bluntness and overall noise reduction for a range of porous plates is presented. The porosity of these flat plates are caused by perforations, or holes, cut into them by a laser cutter. The plates are designed with hole geometries and spacing to fit three groups of dimensionless porosity parameter δ , and results of spectra and OSPL for various Reynolds numbers are presented. Bluntness vortex shedding noise is present at St = 0.20, and the highest porosity plates can reduce this noise by up to 20 dB, effectively removing the peak from the spectra. The relationship between hole shape and noise spectra is complex, where the plates with circular holes were better in general at reducing the bluntness noise peak; however, the plates with aligned holes attenuated low frequency noise slightly better than plates with offset holes at most flow speeds. With increasing porosity, regardless of shape or hole alignment, came an increase in high frequency roughness noise due to the many surface elements (i.e., holes or pores) acting as noise sources. Also, directivity plots help to visualize the small reductions in OSPL and show trends towards the dipole shape with increasing porosity. Lastly, a directivity plot of the SPL at a bluntness noise peak St = 0.20 for a given U_0 shows increasing noise attenuation with increasing porosity. Future work will focus on the same set of plates, characterized by the δ parameter, with sharp TEs, and their resulting effects on the turbulent-boundary-layer TE noise; preliminary results have been published in [27]. Flow field measurements will seek to understand the relationship between the holes and the presence of roughness noise.

Acknowledgments

The authors acknowledge the support of the Fulbright Program, the German-American Fulbright Commission, The Germanistic Society of America, and NSF CAREER award 1846852. The authors would also like to thank Stefan Rohark and Michael Moore for their assistance with manufacturing the experimental setup and the porous plates.

References

- [1] Sarradj, E., Fritzsche, C., and Geyer, T. F., "Silent owl flight: bird flyover noise measurements," *AIAA Journal*, Vol. 49, No. 4, 2011, pp. 769–779.
- [2] Jaworski, J. W., and Peake, N., "Aerodynamic noise from a poroelastic edge with implications for the silent flight of owls," *Journal of Fluid Mechanics*, Vol. 723, 2013, pp. 456–479.

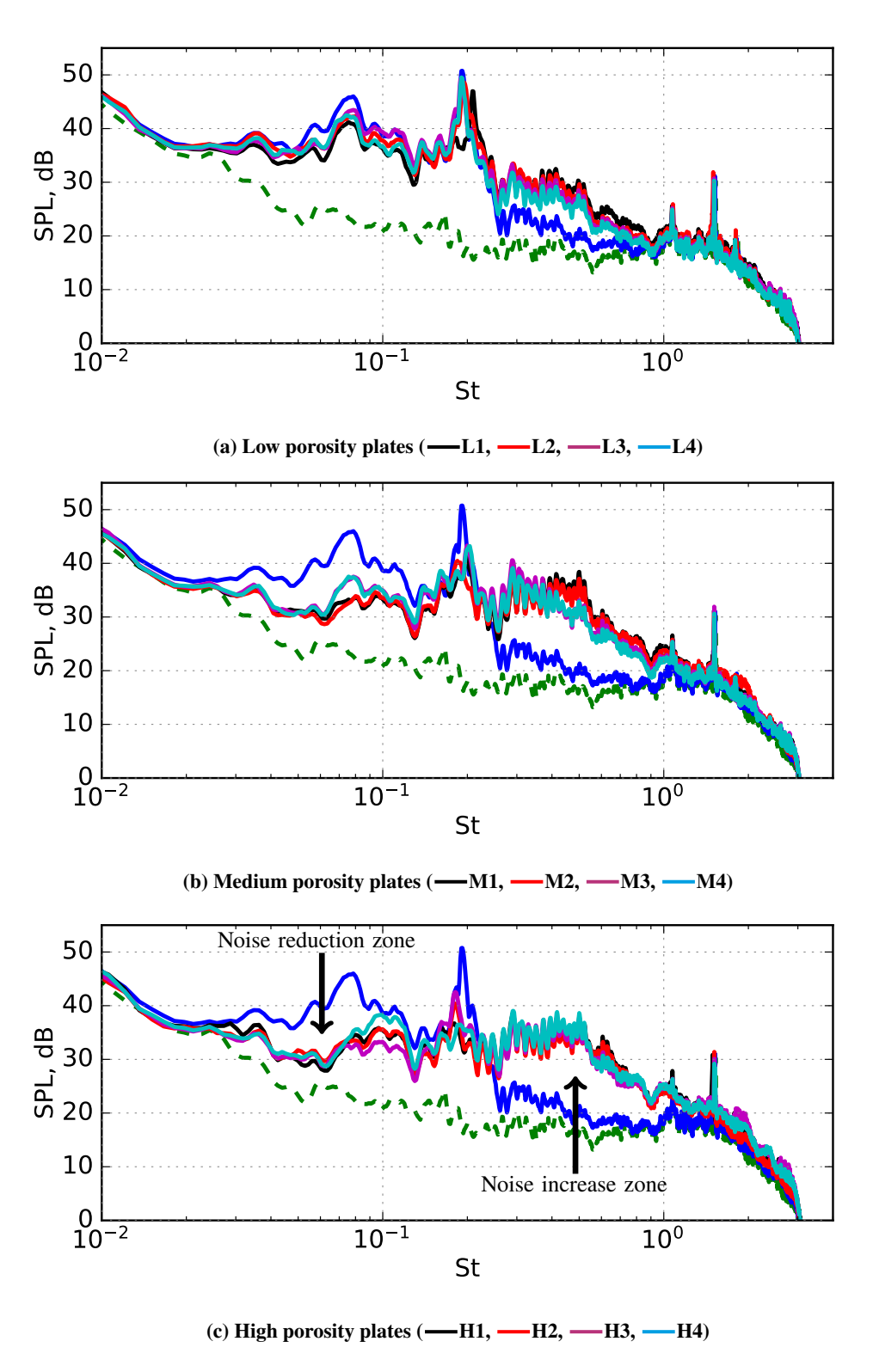


Fig. 7 Dependence of sound pressure level on Strouhal number at $U_0 = 25 \text{ m/s}$ for (a) low, (b) medium, and (c) high porosity plates compared to background noise of empty tunnel (—) and impermeable plate (—).

[3] Jaworski, J. W., and Peake, N., "Aeroacoustics of silent owl flight," Annual Review of Fluid Mechanics, Vol. 52, No. 1, 2020, pp.

- 395-420.
- [4] Chen, H., Yoas, Z. W., Jaworski, J. W., and Krane, M. H., "Acoustic emission of a vortex ring near a porous edge. Part 1: theory," *Journal of Fluid Mechanics*, Vol. 941, 2022.
- [5] Howe, M., "On the added mass of a perforated shell, with application to the generation of aerodynamic sound by a perforated trailing edge," *Proceedings of the Royal Society of London A*, Vol. 365, No. 1721, 1979, pp. 209–233.
- [6] Khorrami, M. R., and Choudhari, M. M., "Application of passive porous treatment to slat trailing edge noise," Tech. Rep. NASA/TM-2003-2 1241, NASA, 2003.
- [7] Geyer, T. F., Sarradj, E., and Fritzsche, C., "Measurement of the noise generation at the trailing edge of porous airfoils," *Experiments in Fluids*, Vol. 48, No. 2, 2010, pp. 291–308.
- [8] Geyer, T. F., and Sarradj, E., "Trailing edge noise of partially porous airfoils," 20th AIAA/CEAS Aeroacoustics Conference, 2014. AIAA Paper 2014-3093.
- [9] Hajian, R., and Jaworski, J. W., "The steady aerodynamics of aerofoils with porosity gradients," *Proceedings of the Royal Society A*, Vol. 473, No. 2205, 2017. 20170266.
- [10] Baddoo, P. J., Hajian, R., and Jaworski, J. W., "Unsteady aerodynamics of porous aerofoils," *Journal of Fluid Mechanics*, Vol. 913, 2021. A16.
- [11] Ayton, L. J., Colbrook, M., Geyer, T. F., Chaitanya, P., and Sarradj, E., "Modelling chordwise-varying porosity to reduce aerofoil-turbulence interaction noise," *AIAA Aviation Forum*, 2021. AIAA Paper 2021-2190.
- [12] Ayton, L. J., Colbrook, M. J., Geyer, T. F., Chaitanya, P., and Sarradj, E., "Reducing aerofoil-turbulence interaction noise through chordwise-varying porosity," *Journal of Fluid Mechanics*, Vol. 906, 2021, p. A1.
- [13] Jiang, C., "Noise generation by airfoils and rotors with porous and serrated trailing edges," Ph.D. thesis, The University of New South Wales, 2020.
- [14] Chung, J., and Blaser, D., "Transfer function method of measuring in-duct acoustic properties. I. Theory," *The Journal of the Acoustical Society of America*, Vol. 68, No. 3, 1980, pp. 907–913.
- [15] Chung, J., and Blaser, D., "Transfer function method of measuring in-duct acoustic properties. II. Experiment," The Journal of the Acoustical Society of America, Vol. 68, No. 3, 1980, pp. 914–921.
- [16] Moreau, D. J., and Doolan, C. J., "Noise-reduction mechanism of a flat-plate serrated trailing edge," AIAA journal, Vol. 51, No. 10, 2013, pp. 2513–2522.
- [17] Showkat Ali, S. A., Azarpeyvand, M., and da Silva, C. R. I., "Trailing edge bluntness noise reduction using porous treatments," Journal of Sound and Vibration, Vol. 474, 2020. 115257.
- [18] Ffowcs Williams, J., and Hall, L., "Aerodynamic sound generation by turbulent flow in the vicinity of a scattering half plane," *Journal of Fluid Mechanics*, Vol. 40, No. 4, 1970, pp. 657–670.
- [19] Ffowcs Williams, J. E., "The acoustics of turbulence near sound-absorbent liners," *Journal of Fluid Mechanics*, Vol. 51, No. 4, 1972, pp. 737–749.
- [20] Yoas, Z., "Passive trailing edge noise attenuation with porosity, inspired by owl plumage," Master's thesis, The Pennsylvania State University, 2021.
- [21] Swann, M., Yoas, Z., Trzcinski, P., Nickels, A., and Krane, M., "Array Processing of Porous Trailing Edge Aeroacoustics," *Bulletin of the American Physical Society*, 2022.
- [22] Sarradj, E., Fritzsche, C., Geyer, T. F., and Giesler, J., "Acoustic and aerodynamic design and characterization of a small-scale aeroacoustic wind tunnel," *Applied Acoustics*, Vol. 70, No. 8, 2009, pp. 1073–1080.
- [23] Geyer, T. F., and Enghardt, L., "Noise generation by two staggered circular cylinders of equal diameter in cross-flow," 28th AIAA/CEAS Aeroacoustics 2022 Conference, 2022. AIAA paper 2022-3093.
- [24] Sarradj, E., and Herold, G., "A Python framework for microphone array data processing," Applied Acoustics, Vol. 116, 2017, pp. 50–58.

- [25] Welch, P., "The use of fast Fourier transform for the estimation of power spectra: a method based on time averaging over short, modified periodograms," *IEEE Transactions on audio and electroacoustics*, Vol. 15, No. 2, 1967, pp. 70–73.
- [26] Vathylakis, A., Chong, T. P., and Joseph, P. F., "Poro-serrated trailing-edge devices for airfoil self-noise reduction," *AIAA Journal*, Vol. 53, No. 11, 2015, pp. 3379–3394.
- [27] Kershner, J. R., Geyer, T. F., and Jaworski, J. W., "Setup for experimental study of porous plate acoustics and local flow features," *Fortschritte der Akustik DAGA 2023*, 2023, pp. 530–533.

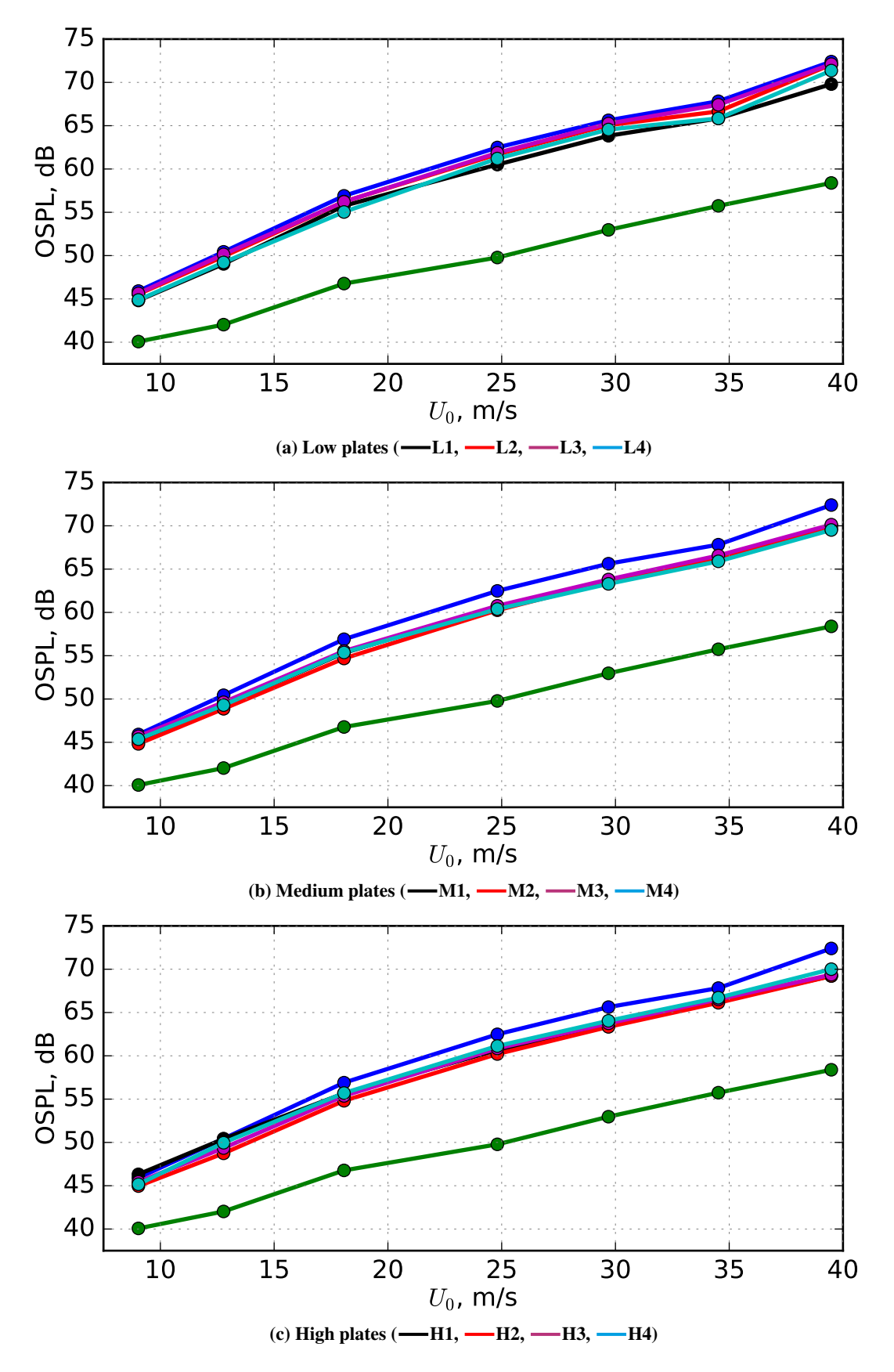


Fig. 8 Dependence of overall sound pressure level on freestream flow speed for (a) low, (b) medium, and (c) high porosity plates, as compared to the background noise of empty tunnel (—) and impermeable plate (—)

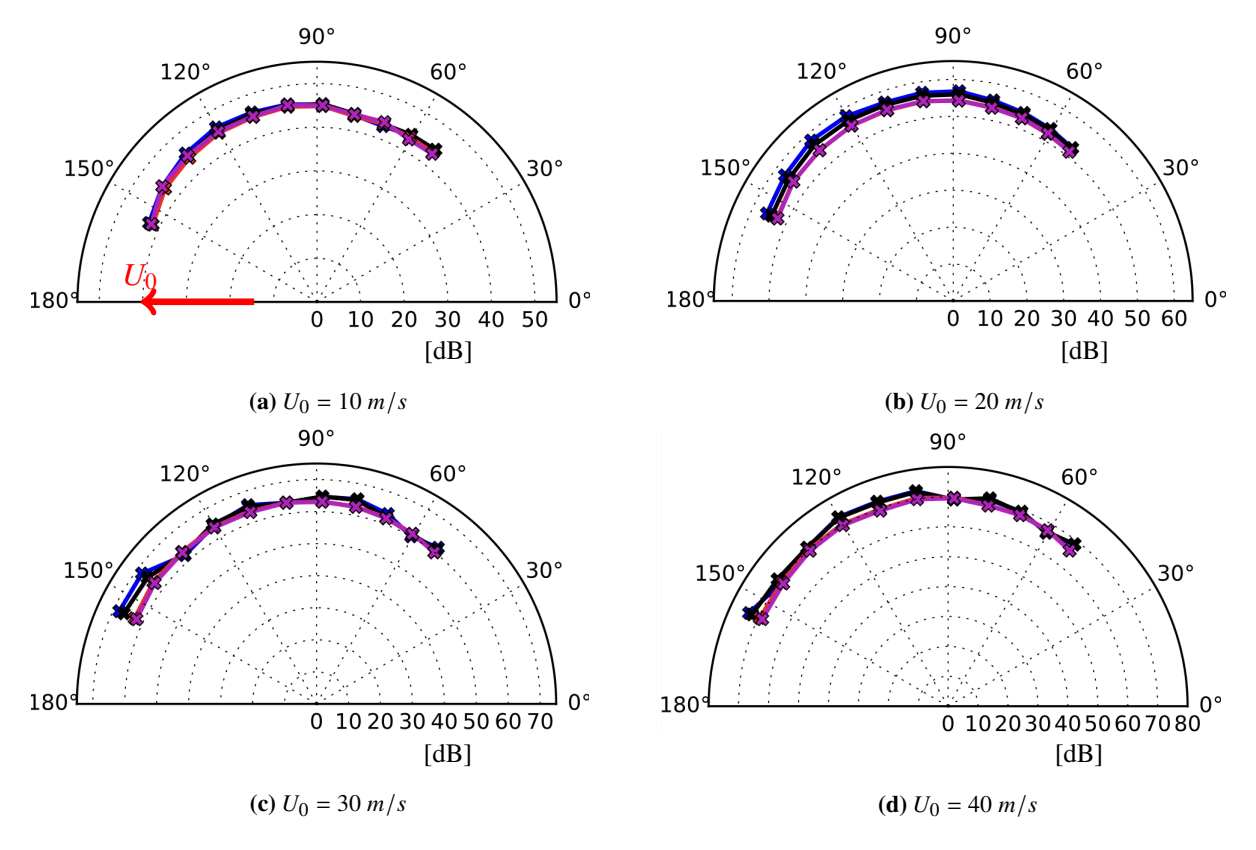


Fig. 9 OSPL of the acoustic waves generated by the trailing edge for each radially-spaced microphone (see Fig. 3) at different speeds and porosity treatments. Impermeable plate (--), L2 plate (--), M2 plate (--), and H2 (--).

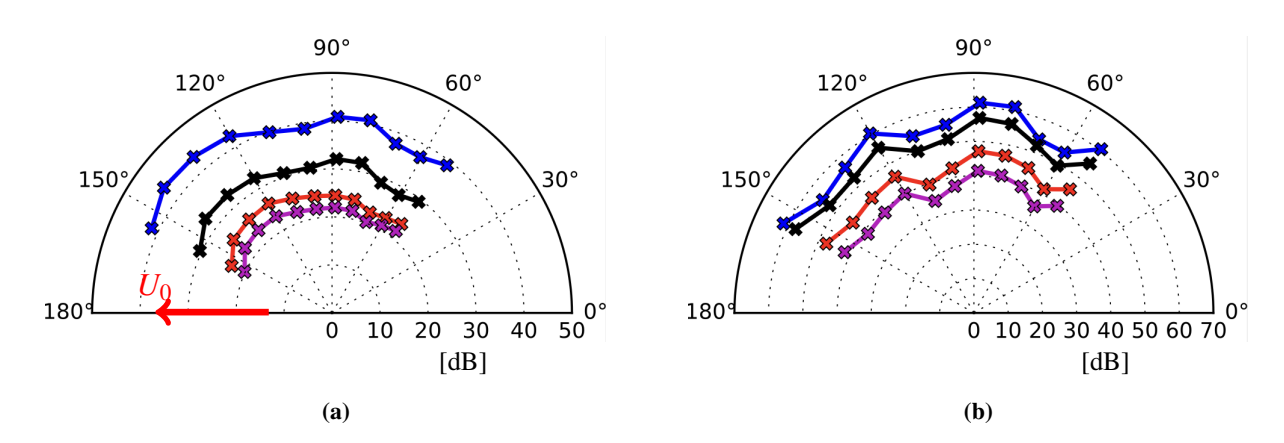


Fig. 10 Directivity of the acoustic waves generated at the trailing edge for each radially spaced microphone at bluntness noise peak, St = 0.2 for (a) $U_0 = 15$ m/s and (b) $U_0 = 35$ m/s. Impermeable plate (—), L2 plate (—), M2 plate (—), and H2 (—).